On the Assessment of a Cooling Tower Scheme for High-Resolution Numerical Weather Modeling for Urban Areas

MIAO YU

Institute of Urban Meteorology, China Meteorological Administration, and State Key Laboratory of Severe Weather, Chinese Academy of Meteorological Sciences, Beijing, China

JORGE GONZÁLEZ

Department of Mechanical Engineering, and NOAA Cooperative Science Center for Earth System Sciences and Remote Sensing Technologies, City College of New York, New York, New York

SHIGUANG MIAO

Institute of Urban Meteorology, China Meteorological Administration, Beijing, China

PRATHAP RAMAMURTHY

Department of Mechanical Engineering, and NOAA Cooperative Science Center for Earth System Sciences and Remote Sensing Technologies, City College of New York, New York, New York

(Manuscript received 8 May 2018, in final form 1 April 2019)

ABSTRACT

A cooling tower scheme that quantifies the sensible and latent anthropogenic heat fluxes released from buildings was coupled to an operational forecasting system [Rapid Refresh Multiscale Analysis and Prediction of the Beijing Urban Meteorological Institute (RMAPS-Urban)] and was evaluated in the context of the megacity of Beijing, China, during summer months. The objective of this scheme is to correct for underestimations of surface latent heat fluxes in regional climate modeling and weather forecasts in urban areas. The performance for surface heat fluxes by the modified RMAPS-Urban is greatly improved when compared with a suite of observations in Beijing. The cooling tower scheme increases the anthropogenic latent heat partition by 90% of the total anthropogenic heat flux release. Averaged surface latent heat flux in urban areas increases to about 64.3 W m^{-2} with a peak of 150 W m^{-2} on dry summer days and 40.35 W m^{-2} with a peak of 150 W m^{-2} on wet summer days. The model performance of near-surface temperature and humidity is also improved. Average 2-m temperature errors are reduced by 1°C, and maximum and minimum temperature errors are improved by 2°–3°C; absolute humidity is increased by 5%.

1. Introduction

The world's population is increasingly urbanized, and much of the urbanization occurs in developing countries (Haub 2010). Land-use change and anthropogenic heat emissions induced by urbanization have been recognized as important factors that have serious impacts on climate at regional scales (Li et al. 2004; Li et al. 2013; Roth 2007). There is ample evidence indicating that the regional climate effect of urbanization is significant (Kalnay and Cai 2003; Kalnay et al. 2006; Hu et al. 2010; Miao et al. 2009; Zhou et al. 2004). Urban impacts are also becoming more and more important in high-resolution weather forecasting as most of the economic wealth is concentrated in cities.

A consequential challenge is discerning the impact of land-use change and anthropogenic heat emissions on regional climates from observations. Numerical models have been used to address this problem (Chen et al. 2011). Anthropogenic heat is a key contributor to the urban heat islands that destroys the near-surface inversion and increases the stratification instability (Allen et al. 2011). Anthropogenic heat release modifies the surface energy balance (Ichinose et al. 1999; Hinkel and

Corresponding author: Miao Yu, yumiao0926@126.com

DOI: 10.1175/JAMC-D-18-0126.1

Nelson 2007). Waste heat released from buildings in cities is a key contributor of anthropogenic heat release (Zheng and Liu 2008). Sailor (2011) provides a historical perspective on the development of models accounting for urban energy consumption and anthropogenic impacts on the urban energy balance.

It has also been indicated that there is a positive feedback cycle: higher temperatures result in increased energy use for indoor air cooling in most urban areas, which in turn increases outdoor near-surface air temperature (Crutzen 2004; Olivo et al. 2017; Salamanca et al. 2014). Furthermore, analysis of global modeling results indicate that heat release from buildings is the largest contributor (89%–96%) from large-scale urban consumption of energy (Allen et al. 2011). Future climate experiments by global circulation models (GCMs) have shown that anthropogenic heat flux can cause annual-mean warming of 0.4°–0.9°C over large industrialized regions, although global-mean anthropogenic heat flux is small (Flanner 2009). Global models have shown that the extra heat from energy consumption over 86 major metropolitan areas can cause up to 1°C of global warming in winter (G. Zhang et al. 2013). The amount of anthropogenic heat released from all sources at night is lower than that during the day, but the temperature increase at night is nearly 3 times that during the day in summer (Narumi et al. 2009). It has also been found that the temperature increased by anthropogenic heat not only depends on the amount of heat releasing from energy but also on geographical and topographical factors (Block et al. 2004).

In the context of regional climate, recent regional climate modeling results have shown that anthropogenic heat flux from buildings has a significant impact on the prediction of near-surface temperatures on urban areas (He et al. 2007). For a study in Tokyo, Japan, the heat release of air conditioning caused about 1°–2°C warming in summer over commercial areas (Ohashi et al. 2007). A study for Paris, France, also indicated an average increase of about 0.5°C in the urban heat island intensity resulted from anthropogenic heat release and pointed out that air conditioning makes important contributions to near-surface warming (de Muncket al. 2013). The modeling study by Feng et al. (2012) for three major urban agglomerations in China suggests that contributions of anthropogenic heat release to warming are larger than the impact of land-use change, which influences surface energy balance. They found that urban land-use change and anthropogenic heat increased the sensible heat flux with amplitudes of up to 20 $W m^{-2}$, while the influence on sensible heat flux attributed to anthropogenic heat is much higher in winter.

Modeling efforts to quantify anthropogenic heat release at regional scales have included single- and multiple-layer urban canopy models. A single-layer urban canopy model (SLUCM) developed by Kusaka et al. (2001) and Kusaka and Kimura (2004) can add the diurnal profile of anthropogenic heat releasing. Other efforts include the Building Effect Parameterization (BEP) and the Building Energy Model (BEM) schemes implemented in WRF that can more accurately describe three-dimensional urban land surface features and processes, including anthropogenic heat from buildings (Martilli et al. 2002; Salamanca et al. 2011).

Despite these advances and evidence of the importance of anthropogenic heat emissions from buildings, the performance of current urban canopy models is unsatisfactory for anthropogenic heat emissions in urban areas (Fan 2015; Feng et al. 2012). The urban canopy model (UCM) developed by Kusaka et al. (2001) can artificially add a diurnal pattern of anthropogenic heating (AH) as an extra source of sensible heat. The BEP developed by Martilli et al. (2002) does not include any type of AH. Neither the UCM nor the BPE has the ability to compute AH release, which may lead to inaccurate simulations of the energy balance.

Early developments of the BEM model have addressed the above challenge to a great extent (Salamanca and Martilli 2010). The current BEM model proposed by Salamanca and Martilli takes into account 1) the heat diffusion through walls, roofs, and floors of the buildings; 2) the natural ventilation and the radiation exchanged between the indoor surfaces; 3) the heat from occupants and equipment; and 4) the energy consumption from air conditioning. Although BEM has the ability to simulate the building energy exchange process as mentioned above, the performance is not satisfactory enough, particularly for high-resolution forecasts in very dense urban areas (Fan 2015; Li et al. 2013; Barlage et al. 2016). One key reason for this performance deficit is the fact that air-conditioning heat release is treated as sensible heat flux in the potential temperature equation when coupled to a regional model such as WRF (Salamanca et al. 2011). The net result is that simulated temperatures in urban areas tend to consistently overestimate observations in most reported studies (Chen et al. 2011; Liao et al. 2014; Yang et al. 2012). An assessment report for the city of Beijing shows that the maximum latent heat flux simulated by WRF–BEP+BEM is only 40 $W m^{-2}$ while the observation is about 230 $W m^{-2}$ (Fan 2015), which directly leads to underestimation of the humidity and further affects the performance of rainfall. In addition, urban fraction and urban morphology parameters may play an important role in determining the sensible and latent heat fluxes in the urban environments. In most commercial buildings, anthropogenic heat can be associated to heat release from air-conditioning systems. Most air-conditioning systems

use evaporative cooling, which releases a mixture of sensible and latent heat to the environment (González and Bula-Silvera 2017).

Many studies have shown that the energy consumption for air conditioning is gradually increasing and correlates with increases in regional temperatures (Adnot 2003). Heat released from the building air-conditioning system is one of the primary sources of anthropogenic sensible and latent heat fluxes in urban areas (Hassid et al. 2000; Akbari et al. 2001; Akbari and Konopacki 2004; Kolokotroni et al. 2006; Salamanca et al. 2011). Previous studies have indicated that heat released from air-conditioning systems in some megacities is equal to or more than one-half of the surface sensible flux (Ohashi et al. 2007). Furthermore, simulation results have shown that the contribution of heat released by air conditioning to summer warming can exceed 1°C in the megacities (Ohashi et al. 2007; Hsieh et al. 2007; Wen and Lian 2009) and contribution to nighttime temperature can reach 2°C (Salamanca et al. 2011).

However, most air-conditioning systems in commercial and high-rise buildings use evaporative cooling, which releases a mixture of sensible and latent heat to the environment. In summer months, 50%–80% of the anthropogenic heat released in commercial and office buildings is through evaporative-cooling systems in the form of latent heat (Sailor et al. 2007). In China, metropolitan electricity consumption reports show that the most important energy consumption in buildings comes from air-conditioning systems whether in commercial or residential areas (Zheng et al. 2015). Air-conditioning usage reports for Chinese metropolitan areas have indicated that the ratio of sensible heat flux to latent heat flux for different types of air-conditioning systems is 20%–80% at the city scale (Zheng et al. 2015).

Thus, how to correctly describe the latent heat flux released by air conditioning in high-resolution models is an urgent modeling challenge that needs to be addressed. It has been shown that a BEM coupled with a cooling tower model can improve the model performance for near-surface temperatures (Gutiérrez et al. 2015). A cooling tower scheme may represent the anthropogenic latent heat flux and may improve the models performance of the energy exchange between a building and its surroundings and the energy balance in the urban boundary layer.

Beijing power consumption has been gradually increasing from 1978 to 2015 and the proportion of electricity consumed by residents is also gradually increasing (Beijing Municipal Bureau of Statistics; http://edu.bjstats.gov.cn/). It is noteworthy that energy consumption from buildings' air conditioning is probably the most important component of summer electricity consumed by residents in summer in Beijing. Consequently, heat flux released by air-conditioning systems in the case of the Beijing urban area becomes one of the primary sources of summer anthropologic heat, and the same can be expected in other large cities. In this study, the simulation of heat flux released by air conditioning was modified using the new cooling tower scheme proposed by Gutiérrez et al. (2015) and it was coupled to the Rapid Refresh Multiscale Analysis and Prediction of the Beijing Urban Meteorological Institute (IUM) (RMAPS-Urban) (Fan 2015).

Our specific goals of this contribution are as follows: 1) to improve the performance of BEM using the new computing method of air-conditioning heat release with partitions for latent and sensible components and 2) to evaluate the forecast performance of improved BEM coupled with RMAPS-Urban for Beijing.

The article is organized as follows: Details of the data and the experimental design are described in section 2. Assessment of the model performance appears in section 3, and we summarize the findings and discuss the results in section 4. The study is a direct result of the urban field study referred to as the Study of Urban Impacts on Rainfall and Fog/Haze (SURF; Liang et al. 2018), which has produced a wealth of high-quality observations for analysis and model performance improvements for weather forecasting in Beijing.

2. Data, model description, and experimental design

The near-surface temperature and humidity data (2 m) were obtained from 294 meteorological stations operated by the Beijing Meteorological Bureau (Fig. 1b). Vertical temperature data were obtained from microwave radiometers (TP/WVP-3000) located in an urban station (Nanjiao, located at 39.8°N, 116.46°E) and a rural station (Yanqing, located at 40.45°N, 115.97°E) (Fig. 1b). Heat flux data (140 m) used in this study were obtained from the Beijing meteorological tower (39.97°N, 116.37°E), which is 325 m high and is located in north Beijing.

This study used operational RMAPS based on a modified version of the WRF Model (ARW, version 3.5.1; Skamarock et al. 2008) and its data assimilation system (WRFDA, version 3.5) developed by the IUM (Fan 2015). The RMAPS system starts with European Centre for Medium-Range Weather Forecasts (ECMWF) global forecasts (at 3-h intervals; 0.25° × 0.25°) and terminates with hourly weather forecasts. Initial conditions are adjusted by WRFDA-ingested including S/C-band weather radar, Ground-Based Global Positioning System Meteorology (GPS-MET), radiosonde, Aircraft Meteorological Data Relay (AMDAR), and automatic weather station (AWS) surface observations. Three domains are designed for the current modeling study with horizontal grid spacings of 9, 3,

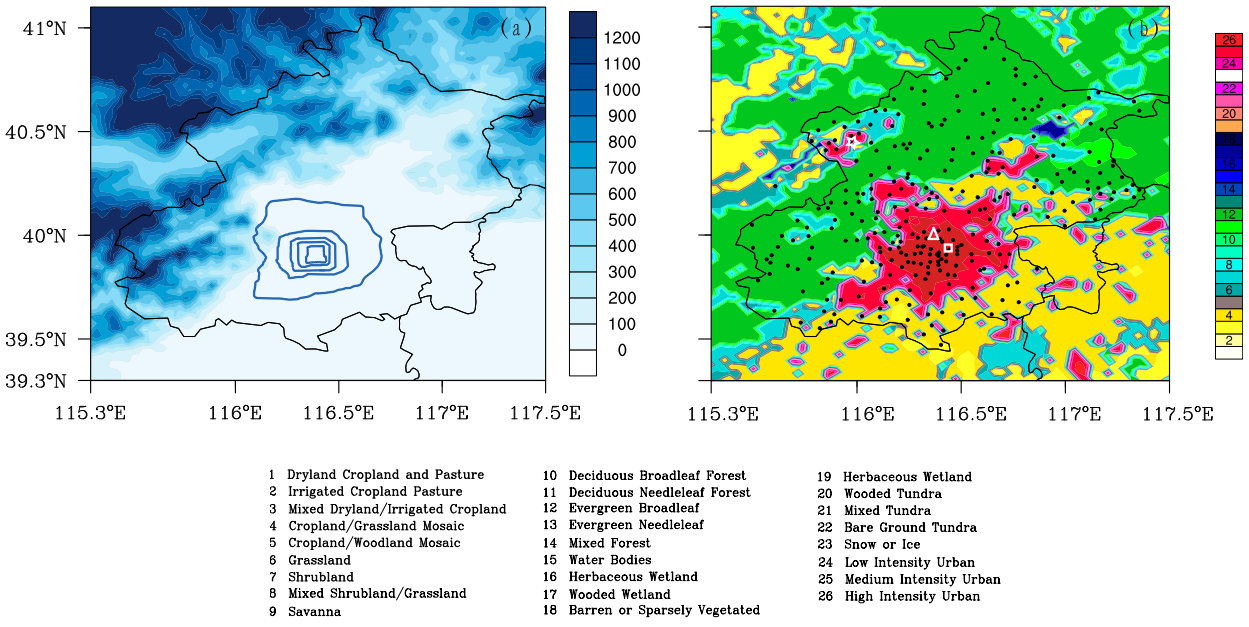

FIG. 1. For RMAPS-Urban: (a) terrain distribution (shading; m)—the blue lines show the second–sixth ring roads—and (b) high-resolution land-use map. In (b), black dots show the 294 weather stations, the triangle shows the location of the 325-m meteorological tower (39.97°N, 116.37°E), the rectangle shows the location of the Naojiao station (39.8°N, 116.46°E), and the star shows the location of the Yanqing station (40.45°N, 115.97°E).

and 1 km. The locations of the nested domains are shown in Fig. 2. Boundary conditions for the 1-km domain-3 model are received from its 3-km output, and variational Doppler radar analysis system (VDRAS) output is assimilated into the 1-km domain via four-dimensional data assimilation (Zhang et al. 2017). Parameterization schemes used in this study are listed in Table 1. The land-use map (Fig. 1) is based on 30-m Landsat data for the year 2010, including three urban land types (Table 2) according to gridded urban-fraction values (Y. Zhang et al. 2013).

To improve the current forecast model, a new cooling tower scheme developed by Gutiérrez et al. (2015) was incorporated into the BEP+BEM and was coupled with RMAPS-Urban. The scheme calculates the heat exchange in evaporative cooling by determining inlet water temperature to the air-conditioning system and outlet air temperature and humidity to the environment. The computing method is as follows:

Based on the first law of thermodynamics, heat exchange equation between the air-conditioning system and the external atmosphere is defined as

$$Q = C_{\min}(T_{\text{wo,cond}} - T_{\text{wi,cond}}) = C_{\min}(T_{\text{Refi}} - T_{\text{wi,cond}}),$$

$$T_{\text{wi,cond}} = T_{\text{wo,CT}} = T_{\text{wb,air}}, \quad \text{and}$$

$$T_{\text{wo,cond}} = T_{\text{wi,CT}},$$

where Q is the heat exchange, which includes the total heat flux in the condenser to maintain the target indoor temperature; $T_{\text{wi,cond}}$ is the water temperature entering the air-conditioning system; $T_{\text{wo,cond}}$ is the water temperature leaving the air conditioner; $T_{\text{wi,CT}}$ is the water temperature entering the cooling system; $T_{\text{wo,CT}}$ is the water temperature leaving the cooling tower (CT); the typical superheated temperature (T_{Refi}) out of the compressor is 60°C; and $C_{\min}$ is the minimum

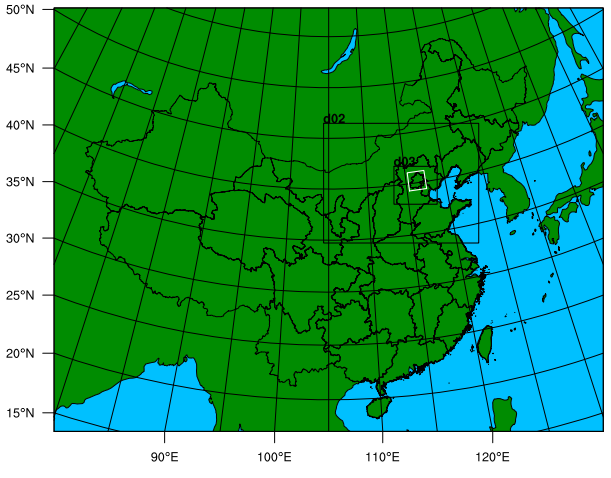

FIG. 2. Domain configuration and location of the study area. The white box is the location of the Beijing area (39.3–41.1°N, 115.3–117.5°E) within domain 3.

TABLE 1. RMAPS-Urban settings and parameterization options for each domain.

	Domain 1	Domain 2	Domain 3
Models and versions	WRFDA v3.5.1 + WRF v3.5.1		WRF v3.5.1
Horizontal grid points	649 × 400	550 × 424	460 × 403
Δx (km)	9	3	1
Vertical layers	50		
Cumulus physics	Kain–Fritsch (Kain 2004)	None	None
Longwave radiation	RRTM (Mlawer et al. 1997)		
Shortwave radiation	Dudhia (Dudhia 1989)		
Microphysics	Thompson (Thompson et al. 2004)		
PBL physics	ACM2 (Pleim 2007)	BouLac (Bougeault and Lacarrere 1989)	
Urban physics	SLUCM (Kusaka et al. 2001)	BEP (Salamanca et al. 2011)	BEP+BEM (Salamanca and Martilli 2010)

thermal capacitance between the water and the refrigerant (González and Bula-Silvera 2017). The air-conditioning systems were assumed to operate 24 h per day. It is assumed that the cooling tower is able to bring the water entering the air-conditioning system to its minimum value of the wet bulb temperature. This wet bulb temperature $T_{\mathrm{wb,air}}$ is calculated from Stull (2011),

$$T_{\mathrm{wb,air}} = T_{\mathrm{air}}\mathrm{atan}[0.151\,977(\mathrm{RH}+8.313\,659)^{1/2}] + \mathrm{atan}(T_{\mathrm{air}}+\mathrm{RH}) - \mathrm{atan}(\mathrm{RH}-1.676\,331) + 0.003\,918\,38\,(\mathrm{RH})^{3/2}\,\mathrm{atan}(0.023\,101\mathrm{RH}) - 4.686\,035,$$

where T_{air} is air temperature and RH is relative humidity in percent.

The efficiency ε for the cooling tower is defined as

$$\varepsilon = \frac{Q}{m_a(h_{\mathrm{sai}} - h_{\mathrm{ai}})},$$

where h_{ai} is the enthalpy of inlet air and h_{sai} is saturated enthalpy of inlet air.

Last, the outlet air temperature T_{ao} can be obtained from the following equations using an iterative scheme:

$$Q = m_a(h_{\mathrm{ao}} - h_{\mathrm{ai}}),$$

$$h_{\mathrm{ao}} = h_{\mathrm{ai}} + \varepsilon(h_{\mathrm{sai}} - h_{\mathrm{ai}}),$$

$$C_p T_{\mathrm{ao}} + q_{\mathrm{vao}}(C_{\mathrm{pw}} + L) = h_{\mathrm{ao}},$$

$$q_{\mathrm{vao}} = 0.621\,98[e/(P-e)], \quad \text{and}$$

$$e = 6.11 \times 10^{7.5T_{\mathrm{ao}}/(237.7+T_{\mathrm{ao}})},$$

where q_{vao} is absolute humidity, or mixing ratio.

This cooling tower scheme parameterizes the anthropogenic heat into sensible and latent by assuming an evaporative-cooling system as a way to remove the heat from the air-conditioning machines. The phase change component of the evaporative process is attributed as latent anthropogenic heat, and the remaining components are attributed as sensible anthropogenic heat flux. The latent and sensible heat fluxes released by the air-conditioning system change the temperature and humidity around the building to achieve the feedback rather than being directly added to the surface flux. This scheme was evaluated by comparing model results with a network of ground based surface weather stations in New York City, New York, with reasonably good results. Although the new cooling tower scheme has been used for the regional model in previous works, verification and evaluation for the improved model were not sufficient, especially for vertical stratification and surface energy fluxes. Previous quantitative evaluations in New York City (Gutiérrez et al. 2015) and Paris (de Munck et al. 2013) were evaluated against near-surface

TABLE 2. Distribution (%) of building heights (m) for three urban land-use types, along with the corresponding urban fraction (%).

	5	10	15	20	25	30	Urban fraction
High-intensity urban	0.0	0.0	10.0	25.0	40.0	25.0	95
Medium-intensity urban	0.0	20.0	60.0	20.0	0.0	0.0	80
Low-intensity urban	15.0	70.0	15.0	0.0	0.0	0.0	50

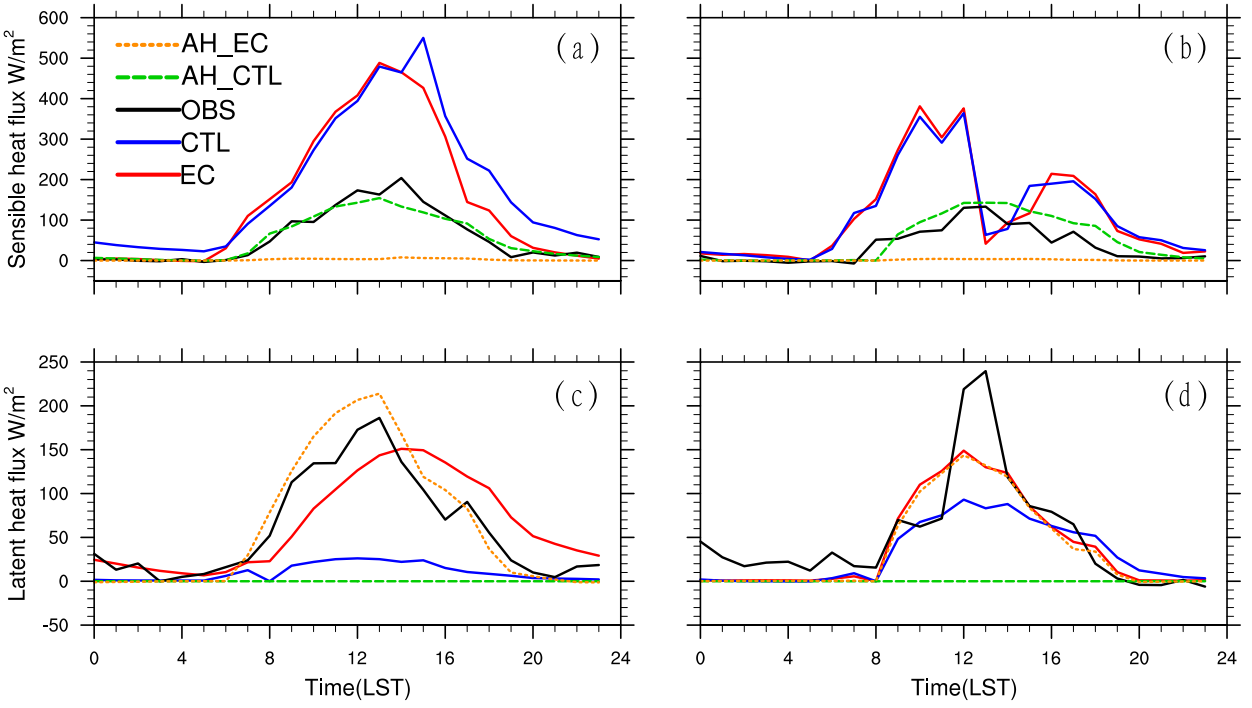

FIG. 3. Averaged diurnal pattern of (a),(b) sensible and (c),(d) latent heat flux ($W\,m^{-2}$) on (left) dry and (right) wet days.

temperature and humidity, mostly because of the lack of observational data for the assessment of surface heat flux and the vertical structure of boundary layer. The present work used multiple intensive periods of observational data from the SURF experiment (Liang et al. 2018) for the evaluation of the possible improvement of the new cooling tower scheme. We choose a two-week period that includes continuous dry days (6–10 July 2005; 10–16 August 2005) and wet days (4–5 July 2005; 17–18 August 2005) to evaluate the performance of the improved RMAPS-Urban (EC). The forecast results by default RMAPS-Urban were used as control runs (CTL).

3. Results

a. Effect on diurnal pattern

The simulated heat flux data were first interpolated to the tower position and used to evaluate to observed tower data. The significant distinction between CTL and EC is in latent heat flux released from buildings because of the EC improvements. The results for the whole study period show that the maximum sensible heat flux from air conditioning in CTL is about $180\,W\,m^{-2}$ (AH_CTL) while it is reduced to $20\,W\,m^{-2}$ in EC (AH_EC) (Figs. 3a,b). Meanwhile latent heat flux from air conditioning is increased (the maximum is increased to $220\,W\,m^{-2}$) by EC in the daytime. Because simulations of the thermal exchange between buildings and their external atmosphere are inadequate in the CTL, surface latent heat flux is less than $20\,W\,m^{-2}$ on dry days (Fig. 3c). EC not only increases the surface latent heat flux releasing from buildings but also improves the ability of the simulation to represent the heat exchange processes.

Next, we evaluate the performance for surface sensible and latent heat fluxes on dry and wet days by comparing modeling and observations. We assumed the turbulent heat fluxes change little with height. Based on the observed heat fluxes by the Beijing tower at 140 m, sensible heat flux is less than $20\,W\,m^{-2}$ in the nighttime, while CTL overestimates sensible heat flux for over about $50\,W\,m^{-2}$ in the nighttime (Fig. 3a). The EC largely corrects this problem during the dry days. However, sensible heat flux on wet days is still overestimated during nighttime for both simulations. In the daytime, observed surface sensible heat flux reaches the maximum ($200\,W\,m^{-2}$) at 1400 LST; both CTL and EC overestimate the sensible heat flux in urban areas (Fig. 3b). Sensible heat flux simulated by CTL delays the time of reaching the maximum by about 1 h, whereas that simulated by EC is an hour earlier than CTL. Both CTL and EC overestimate sensible heat flux in the urban area, but EC improves the simulation results from 1500 to 2000 LST, especially on the dry days. When compared with results for dry days, improvements for sensible heat

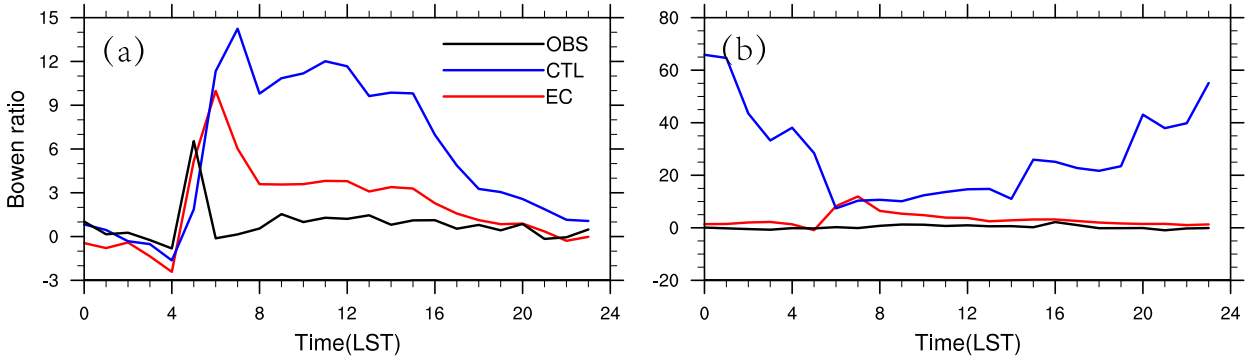

FIG. 4. Averaged diurnal pattern of Bowen ratio for (a) dry and (b) wet days.

flux by ECs on wet days are not that evident (Fig. 3b). Different from the dry days, the sensible heat flux rapidly decreases during 1200–1400 LST in the model results because of rainfall on the wet days. From this, it is evident that simulated sensible heat flux is more sensitive to precipitation than that in observations.

Next, assessment of results for latent heat flux shows that the simulations by CTL are less effective than the EC. The maximum observed latent heat flux is about 200 W m^{-2} while the latent heat flux is seriously underestimated by CTL in the urban area, which furthermore leads to errors in surface humidity and temperature. However, EC results indicate that the model performance for latent heat flux is significantly improved on both dry and wet days (Figs. 3c,d). The simulated diurnal pattern of latent heat flux by EC is very close to the observations, although the value is still slightly less than the observations.

Note that in both the EC and CTL the storage heat flux is not modeled; it is the residual term. However, because of lack of direct measurements of storage heat flux, the feedback between the two fluxes is yet unknown. This underlying gap in knowledge is one of the prime reasons for large root-mean-square errors (RMSEs) in sensible heat flux prediction. Additionally, the flux tower measurements also suffer from advection related to surface heterogeneity and could potentially underestimate the sensible heat flux.

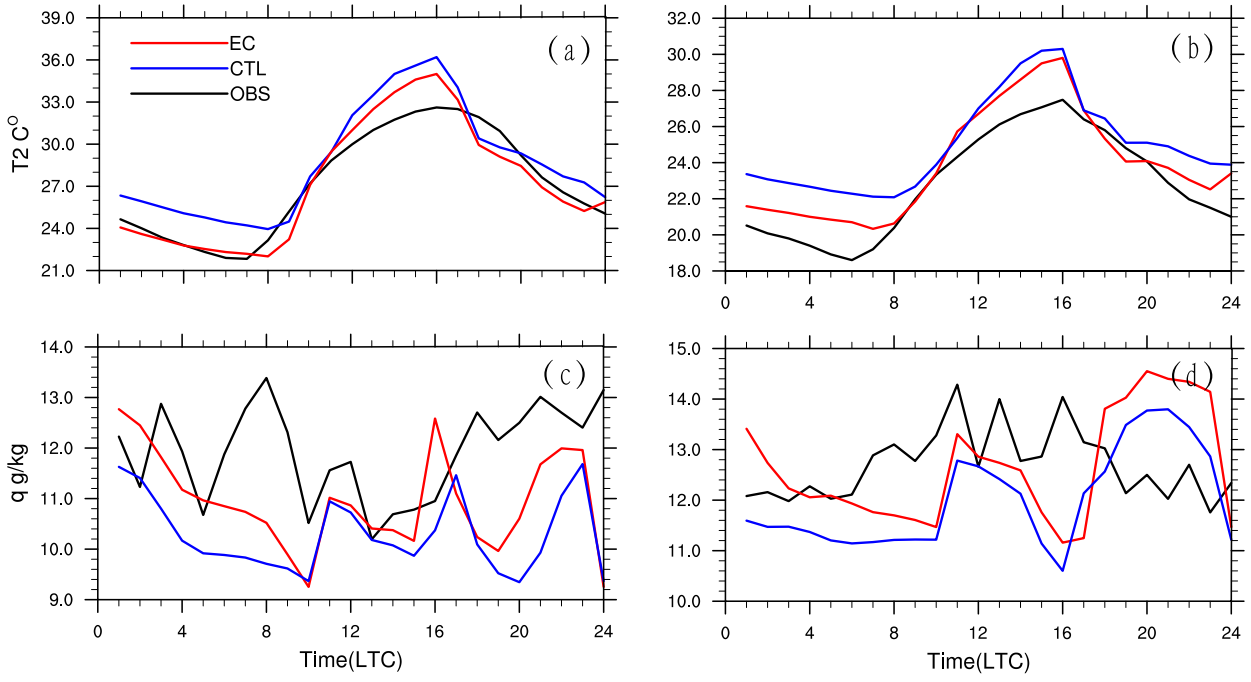

FIG. 5. Average diurnal pattern of (a),(b) temperature (°C) and (c),(d) absolute humidity (g kg^{-1}) in the urban area on (left) dry and (right) wet days.

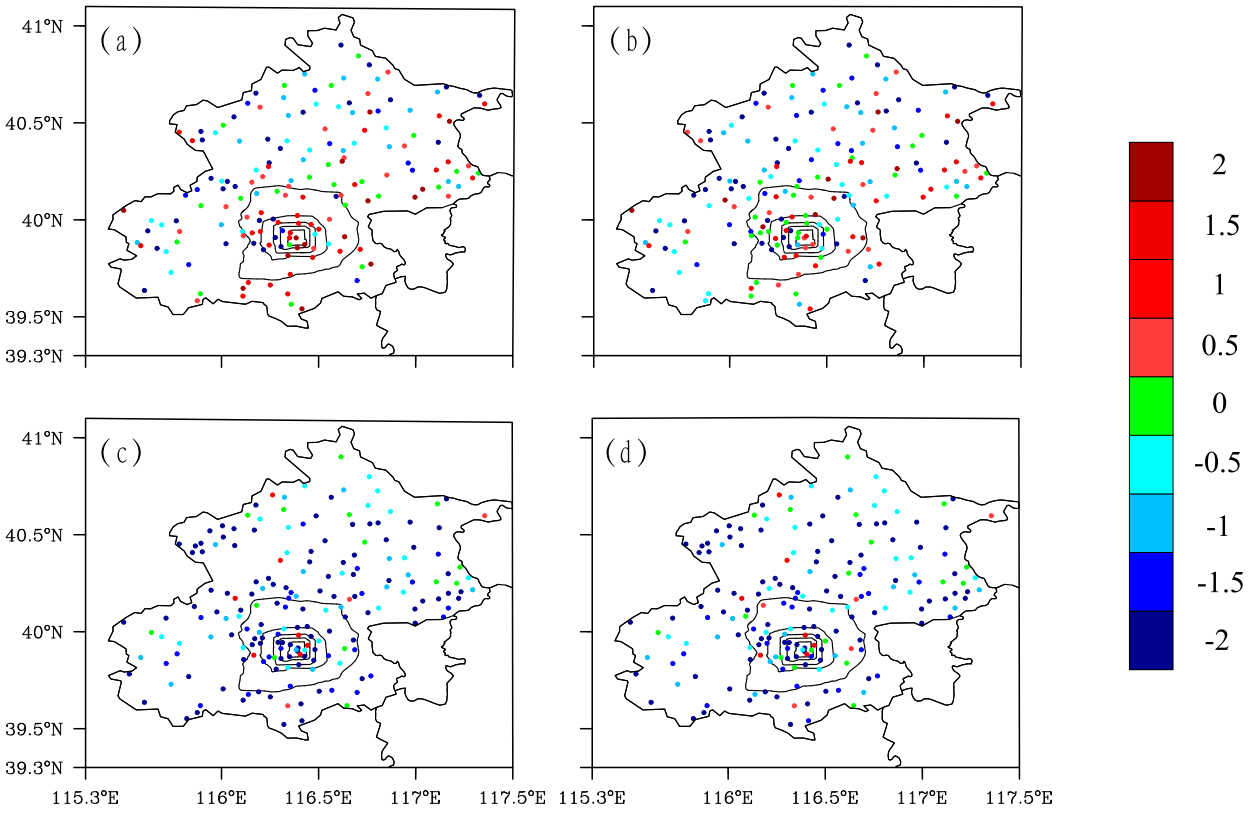

FIG. 6. Spatial distribution of averaged temperature (°C) and absolute humidity (g·kg^{-1}) errors (simulated values minus the observed values) at 2 m: temperature error in (a) RMAPS-Urban and (b) EC and absolute humidity error in (c) RMAPS-Urban and (d) EC.

The Bowen ratio is a very important indicator for the surface energy balance. The Bowen ratio is used to describe the type of heat transfer for a moist surface. It is defined by the following equation:

$$B = Q_h/Q_e,$$

where Q_h is surface sensible heating and Q_e is surface latent heating.

Because the latent heat flux is seriously underestimated by CTL, there are large simulation errors for Bowen ratio especially for nighttime on both dry and rainy days (Fig. 4). The EC results are very encouraging; however, there are still some errors especially from 600 to 900 LST. In the dry day, the observed Bowen ratio is less than 2 for most days except at 500 LST when the Bowen ratio is larger than 6. The CTL overestimated the Bowen ratio with values larger than 4 in daytime and with a delay of 2 h on the timing for observed the maximum Bowen ratio (Fig. 4a). EC, however, improves the simulation of Bowen ratio, especially in daytime with values of less than 4, and also reduces the difference in the timing for maximum Bowen ratio occurrence. On the wet days, the observed Bowen ratio is less than 4 and there are minimal diurnal variations. CTL overestimated the Bowen ratio during the whole day, especially for nighttime, when it gives values that are larger than 30 (Fig. 4b); EC, however, reduces most simulated errors for nighttime, although the Bowen ratio is larger than 5 from 0600 to 900 LST.

The surface heat flux modifications by EC will further influence temperature and humidity in urban areas. We therefore evaluate the model performance for temperature and humidity at 2 m. For the dry days, the surface temperatures are clearly overestimated by CTL for all hours of the day. The model performance is largely improved by EC, especially for nighttime. Averaged temperature at 2 m is decreased by 3°C by EC for nighttime, which is very close to the observation (Fig. 5a). There are still some errors during 1200–1600 LST. For the wet days, improvement for nighttime is still significant (2°) but not as good as for the dry days when compared to the observations (Fig. 5b). For temperature, the root-mean-square error in CTL is 1.29°C on dry days and 1.34°C on wet days, whereas the values are 1.00° and 0.43°C in EC. Although EC improves the overall daily temperature by approximately 1.5°C, the maximum simulation deviation still occurred from 1200

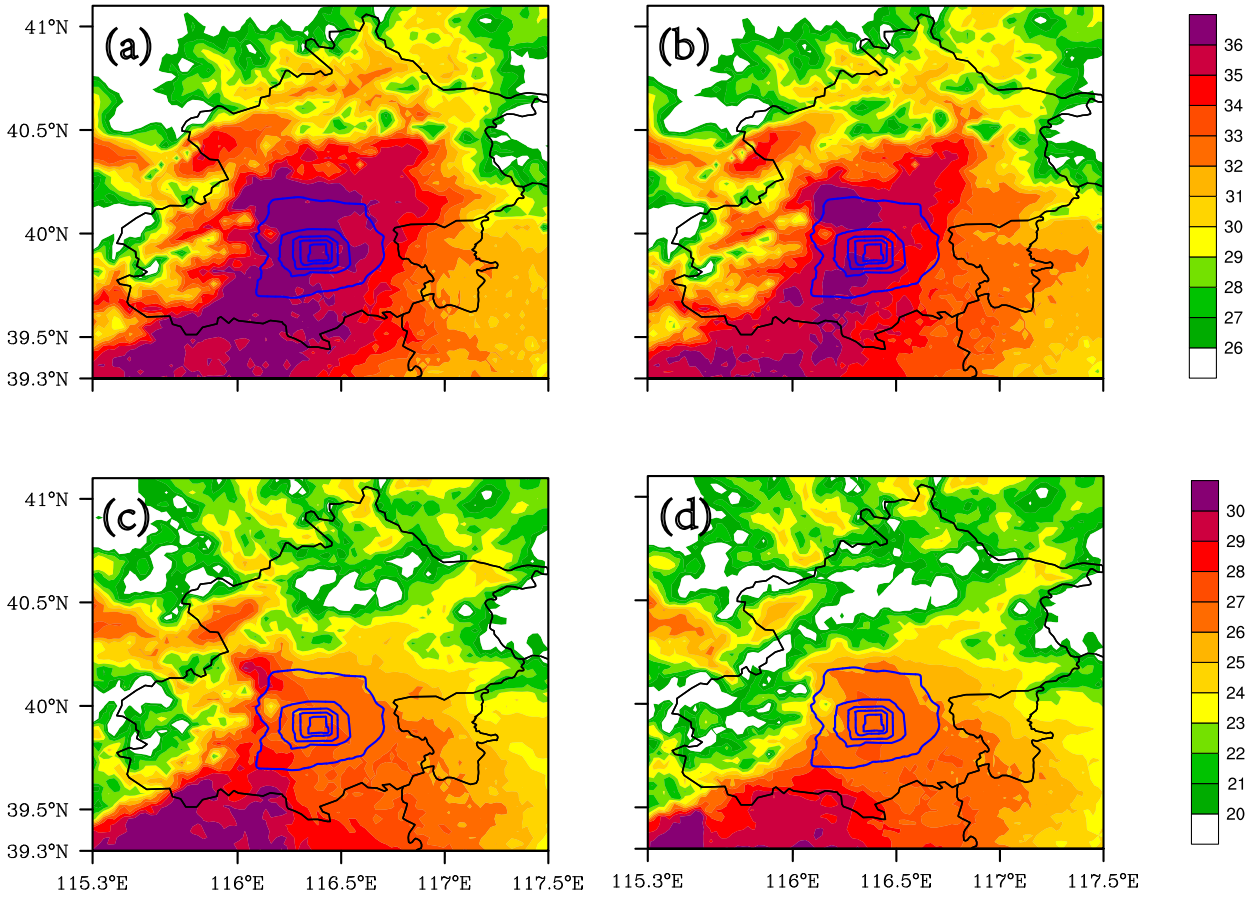

FIG. 7. Spatial distribution of averaged temperature (°C) at 2 m at 1500 LT as simulated by (left) RMAPS-Urban and (right) EC on (a),(b) dry and (c),(d) wet days.

to 1600 LST. That is likely related to overestimation of the sensible heat flux. Another error in simulation is the time of maximum and minimum temperatures. The time of maximum (minimum) of CTL and EC is ahead (behind) the observation by 1 h. This could be due to underestimating the thermal storage of the city.

For the dry days, absolute humidity is underestimated by CTL during the whole day, while it is improved by EC, especially for nighttime (Fig. 5c). For the wet days, absolute humidity increases during 1000–1600, likely because of the rainfall that occurred in this period. For the wet days, simulated absolute humidity in both CTL and EC lags behind the observations and increases from 1800 to 2300 LST (Fig. 5d). The simulated value is improved by EC although the difference of diurnal features between observation and EC is still obviously in both dry and wet days.

b. *Effect on spatial distribution*

Here, the 294 meteorological stations are used to evaluate the spatial distribution of the model performance for surface temperature and humidity. The spatial distribution of averaged errors for temperatures shows that CTL overestimates daily mean temperatures in most of the urban stations (Fig. 6a), with errors in most stations reaching 1°–2°C. This overestimation is consistent with previous studies in Beijing (Chen et al. 2011; Liao et al. 2014; Yang et al. 2012). Errors on surface temperatures are clearly reduced by EC in the urban areas, with mean average errors in about one-half of the stations of less than 0.5° (Fig. 6b). Both CTL and EC underestimate daily mean absolute humidity at most urban stations, and there is no significant difference or improved effect by EC in mean absolute humidity in the urban areas.

Maximum average temperatures (at 1500 LT) simulated by CTL are more than 36°C in the urban and the suburban areas in the dry days, and 34°C in most of the plains (Fig. 7a), while observations were 34°C in the urban areas and 32°C in suburban areas. These maximum temperatures are reduced by about 1°C in EC in both urban and suburban areas, and the areas where

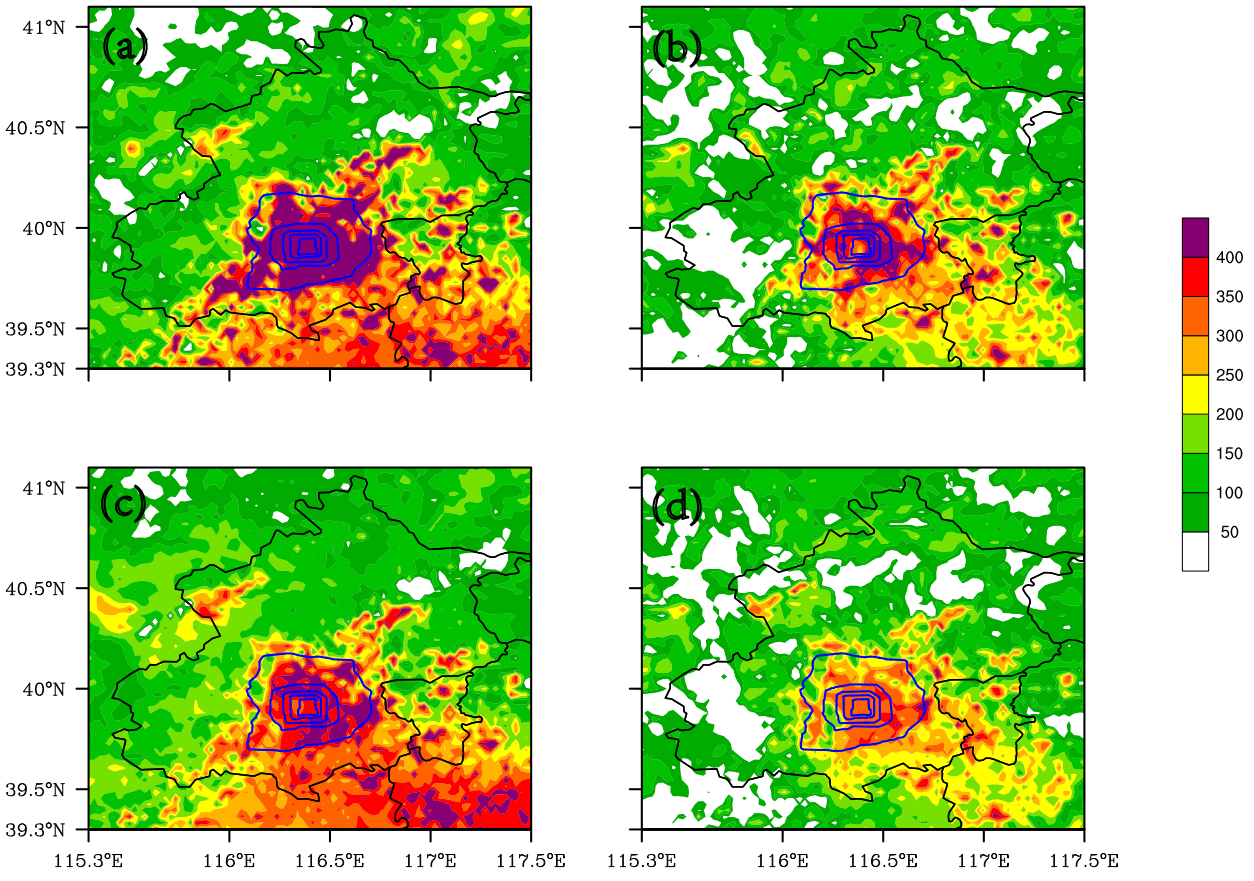

FIG. 8. Spatial distribution of averaged sensible heat flux (W m^{-2}) at 1500 LT as simulated by (a),(b) RMAPS and (c),(d) EC on (left) dry and (right) wet days.

temperatures are more than 36°C clearly decreased (Fig. 7b). These are the same characteristics as for wet days (Figs. 7c,d).

Spatial distribution of maximum sensible heat flux shows that sensible heat flux simulated by CTL in urban areas is more than 400 W m^{-2} on the dry days (Fig. 8a). The sensible heat flux simulated by EC in most urban areas is about 300–400 W m^{-2}, which is smaller than in CTL (Fig. 8c). The maximum region (more than 400 W m^{-2}) of sensible heat flux is obviously reduced by EC. On the wet days, sensible heat flux maximum simulated by EC is also smaller by about 50–100 W m^{-2} than in CTL (Figs. 8b,d).

Maximum surface latent heat flux simulated by CTL is less than 50 W m^{-2} in downtown areas, which is obviously underestimated relative to observations on both dry and wet days (Figs. 9a,b). Simulation of latent heat flux in urban areas by EC improves the value to 100 W m^{-2} on dry days and 150 W m^{-2} on wet days (Figs. 9c,d).

In relation to anthropogenic emission, maximum sensible heat flux released by air-conditioning systems from buildings in CTL is more than 120 W m^{-2} in urban areas (Figs. 10a,b). EC reduces the maximum sensible heat flux on both dry days and wet days (Figs. 10c,d). As expected, the maximum sensible heat flux on dry days is larger than the wet days simulated by EC (Figs. 10c,d). That means sensible heat flux released through air conditioning in EC is affected by the warmer outdoor conditions on dry days, which is an indication of positive feedback to energy consumption from the buildings. Thus, the model performance of the indoor–outdoor exchange is significantly improved by EC.

Latent heat flux released by the air-conditioning system was not included in potential temperature equation when coupled to WRF in CTL. However, in EC the maximum latent heat flux released is more than 140 W m^{-2} on dry days and 80–100 W m^{-2} on wet days (Figs. 11a,b) over urban areas.

c. *Effect on vertical boundary layer structure*

To evaluate the impacts on the boundary layer structure from the latent flux modifications, microwave

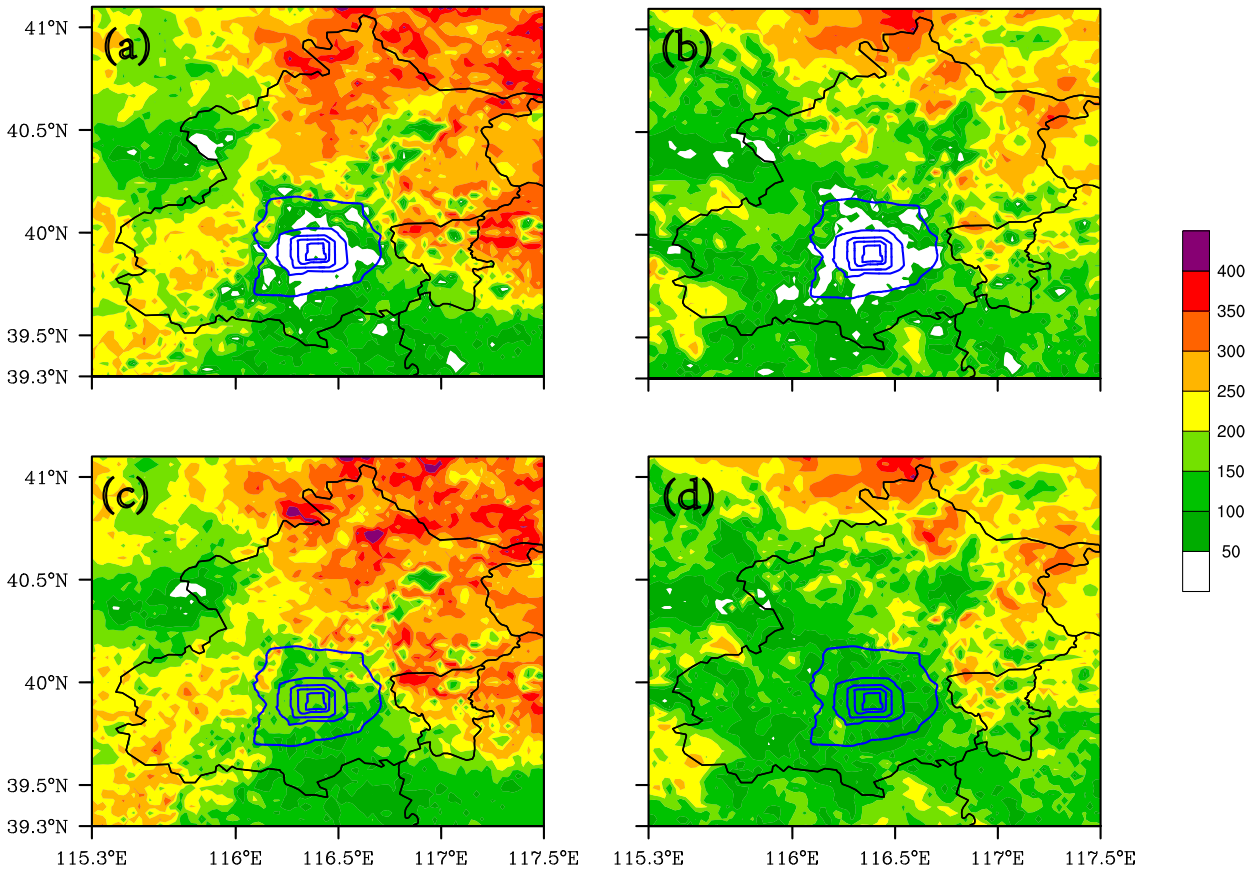

FIG. 9. As in Fig. 8, but for latent heat flux.

radiometer data were used to compare the temperature profiles with model results, as shown in Figs. 12 and 13 . The boundary layer height was about 1 km on dry days in the urban area and the maximum temperature reached 295 K at the top of boundary layer (Fig. 12a). For the wet days, the effect of rainfall on boundary layer structure can reach up to 10 km and the temperature decreases during the rainfall processes (Fig. 12b). Consequently, we did not observe significant improvement in the forecasting of the rainfall events (<5 mm). The simulated vertical temperatures by CTL are overestimated below 6 km from 0800 to 1500 LST, and the error, which reaches 5°C, is most significant in the boundary layer (below 1 km) (Fig. 13a). EC improves the performance on the boundary layer temperatures and shortens the time period of the maximum errors (Fig. 13b). The boundary layer structure of wet day has the same feature as the dry day (Figs. 13c,d). The results could be different when using a different PBL scheme.

Rural and urban potential temperatures vertically descend at 0800 LST, which means the boundary layer is unstable on dry days (Figs. 14a,c). From the observations, at 1400 LST, the boundary is unstable and has a depth of about 800 m (Fig. 14a). The simulated potential temperature profiles by both CTL and EC for both cases during the convective period captures the boundary layer structure below 800 m, but there are errors above 800 m in the urban areas. Although the potential temperature values simulated by both CTL and EC are much higher and the boundary layer height is much deeper than the observations in urban areas, the performance of EC is better than CTL (Figs. 14a,b). For the rural areas, the boundary layer structure becomes neutral (the lapse rate is close to zero) on the dry days. Although the simulated potential temperatures are larger than observations, EC captures the features of the boundary layer structure (Fig. 14c). For the wet days, the observed temperature lapse rates are positive below 200 m both at 0800 and 1400 LST. Simulated boundary layer structure is stable because near-surface temperature is lower than high-level temperature in both 0800 and 1400 LST and near-surface (below 200 m) boundary layer structure was not captured by both CTL and EC. For the rural areas, the simulated vertical boundary layer structures in both

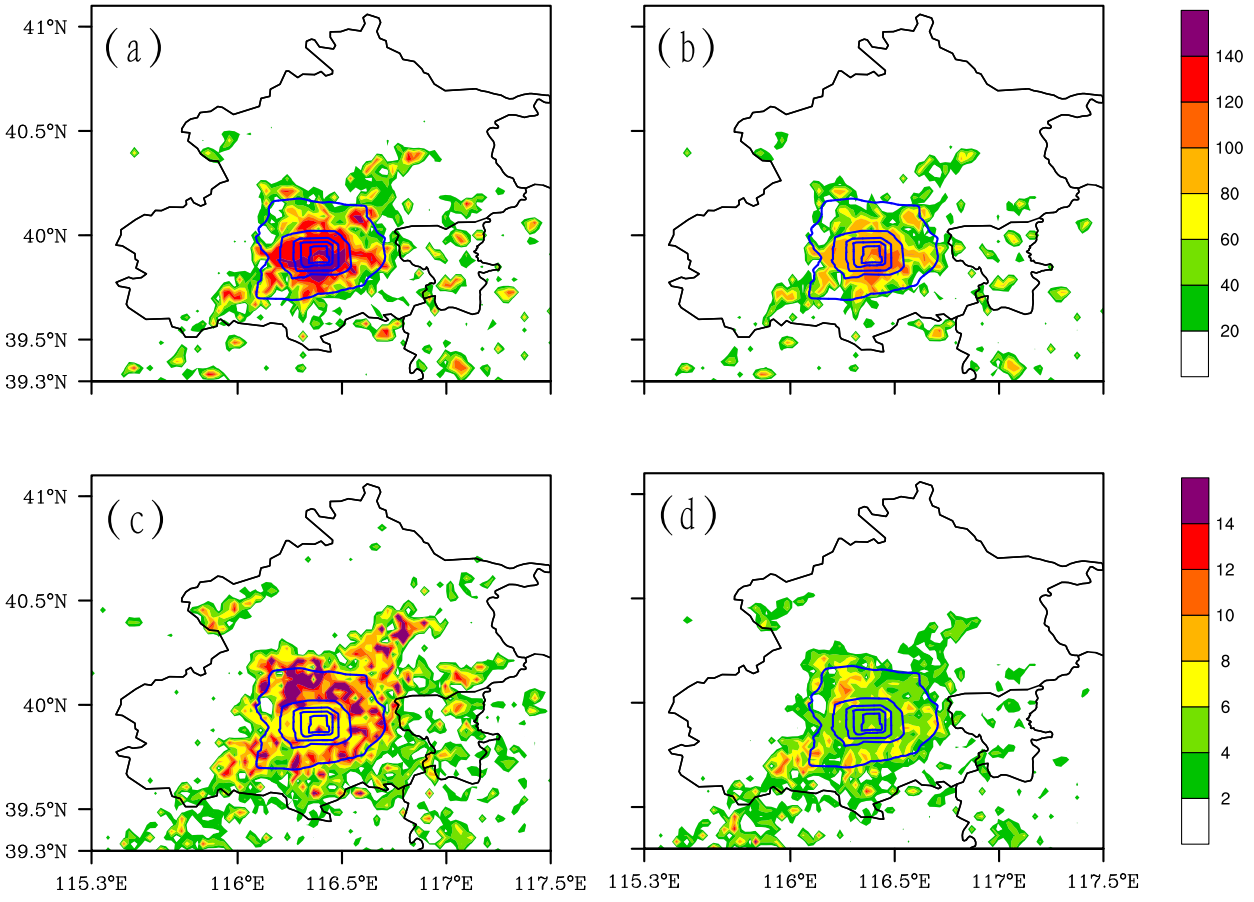

FIG. 10. Spatial distribution of average maximum sensible heat flux (W m^{-2}) released by building air conditioning at 1500 LT as simulated by (a),(b) RMAPS-Urban and (c),(d) EC on (left) dry and (right) wet days.

CTL and EC are very close to the observations on the wet days (Fig. 14d). The rural boundary layer is stable below 1000 m at 0800 LST and neutral at 1400 LST. In general model performance of the boundary layer structure in the rural areas is much better than in the urban areas. This indicates that model errors are mainly due to the representation of the urban processes in the model, including possible inaccuracies in the

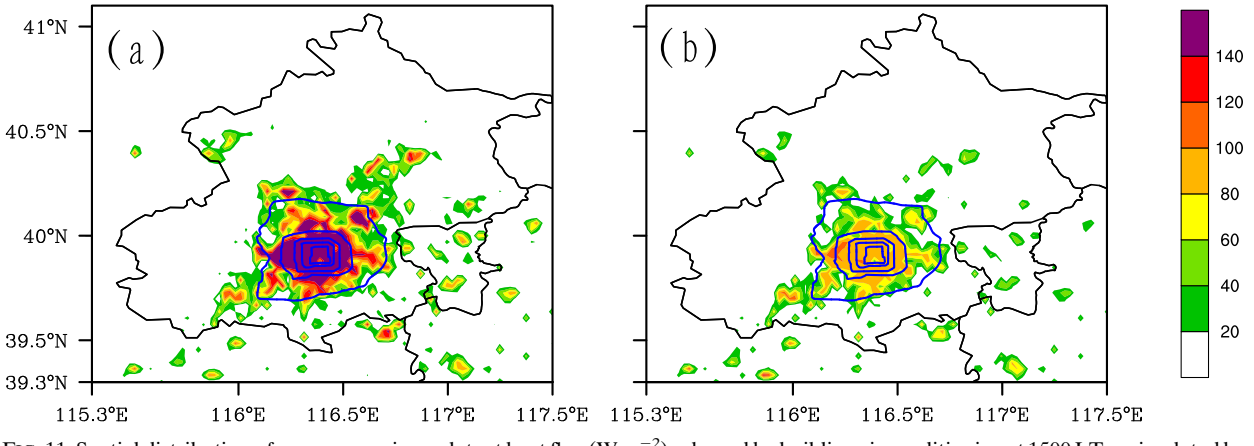

FIG. 11. Spatial distribution of average maximum latent heat flux (W m^{-2}) released by building air conditioning at 1500 LT as simulated by EC on (a) dry and (b) wet days.

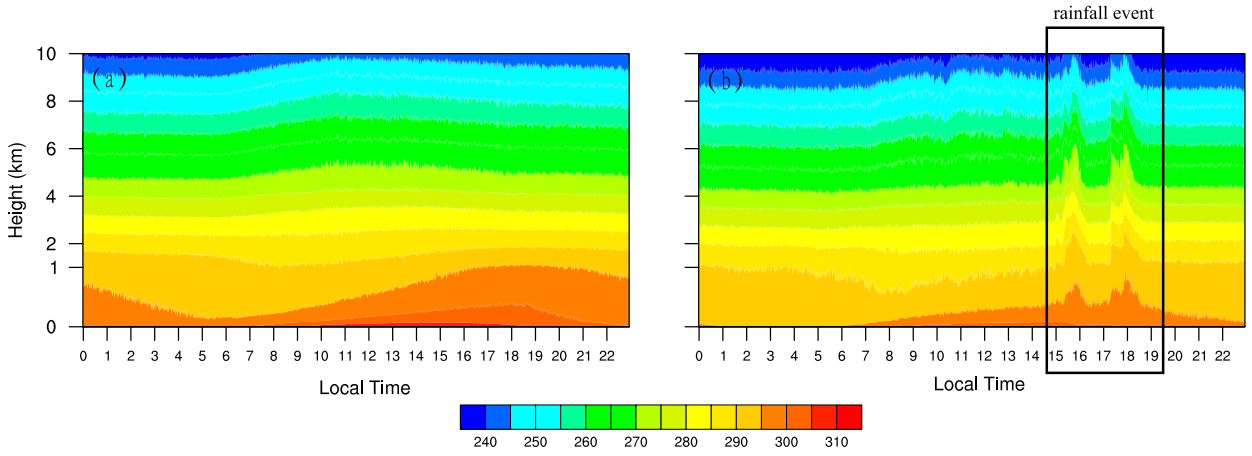

FIG. 12. Averaged vertical temperature profile observed by radiometer (K) on (a) a dry day and (b) a wet day; the black-outlined box in (b) shows the rainfall-event period.

building height data, urban fraction, and boundary layer parameterization schemes.

4. Conclusions and discussion

A new cooling tower scheme is presented that considers the quantitative partition of sensible and latent anthropogenic heat fluxes released from buildings, and it was coupled to RMAPS-Urban and evaluated in the context of the megacity of Beijing during summer months. The computing method is based on the heat and mass transfer between the condenser units and the outdoor inlet air as suggested by Gutiérrez et al. (2015) and is referred to in this study as the cooling tower scheme. The main goal of the introduction of this new scheme is to correct for the underestimation of the latent

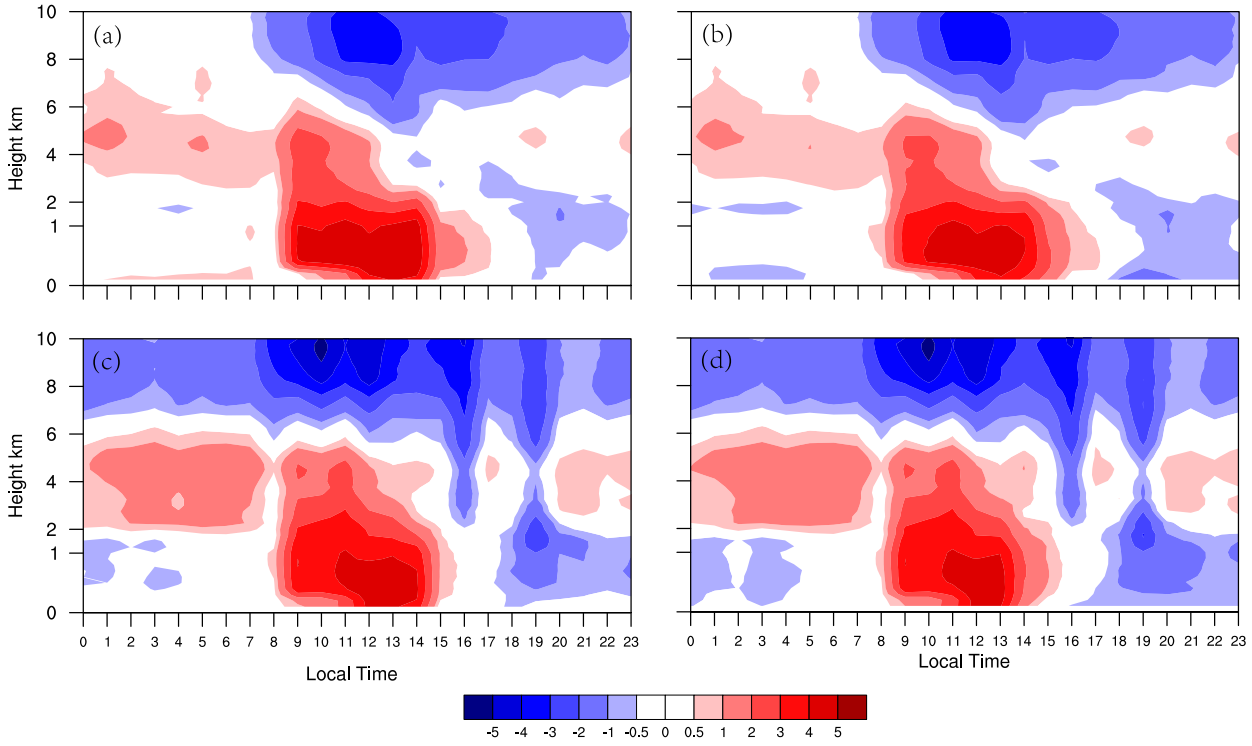

FIG. 13. Difference of averaged vertical temperature profile (K) between modeling and observations as simulated by (left) RMAPS-Urban and (right) EC on (a),(b) dry and (c),(d) wet days.

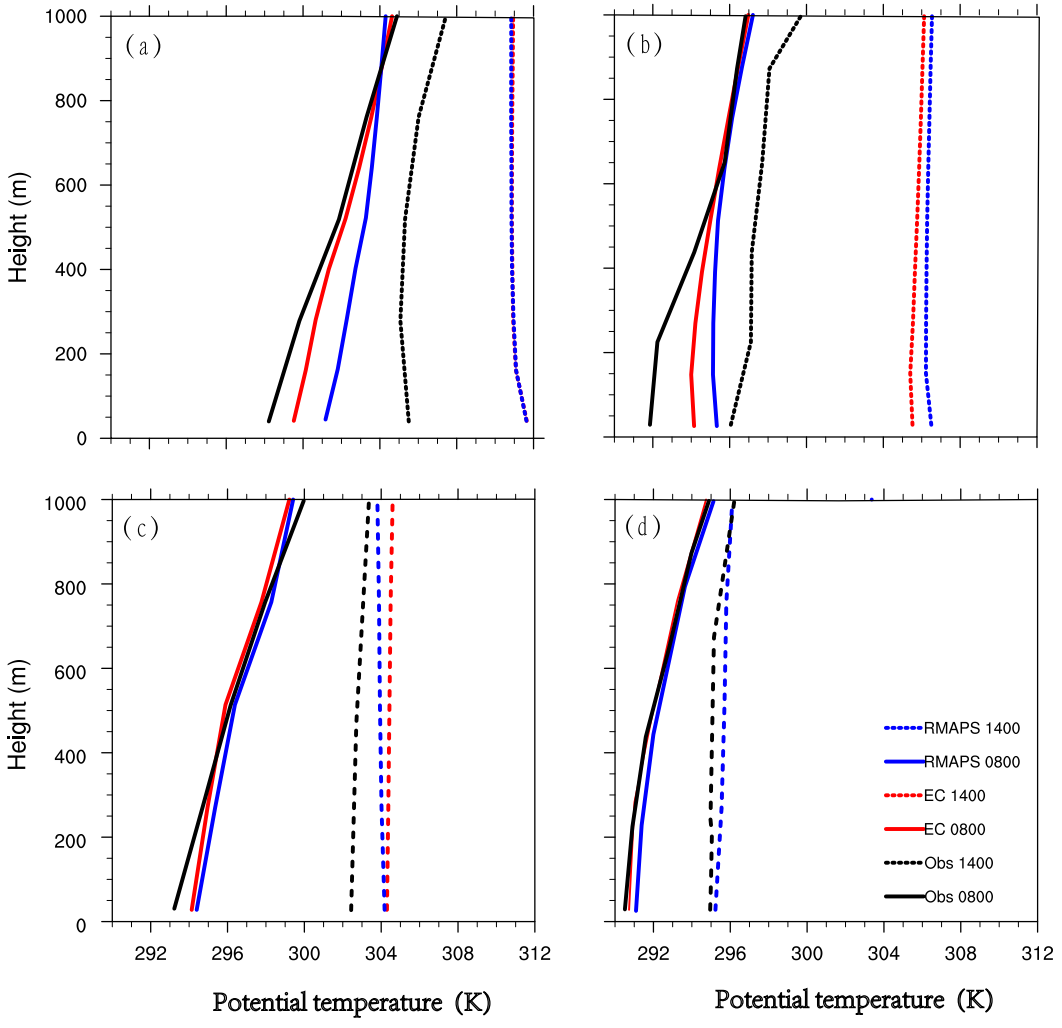

FIG. 14. Potential temperature profile (K) for (a),(b) an urban station and (c),(d) a rural station on (left) dry and (right) wet days.

heat fluxes in urban weather modeling. Two simulations using default RMAPS-Urban (CTL) and improved RMAPS-Urban (EC) estimate the performance of the new scheme, with a focus on dry and wet days. The assessment of the model considers spatial and time series responses in and around the city of Beijing for surface heat fluxes, temperature, and humidity and for performance along the boundary layer. The rich sets of observations were collected as part of the SURF field experiment as described by Liang et al. (2018).

The new cooling tower system in commercial areas not only induces a significant increase in the anthropogenic latent heat partition by 90% of the total heat fluxes released, but also further changes the surface heat flux feature. When the EC is introduced, averaged surface latent heat flux in urban areas increases to about 64.3 $W m^{-2}$ (40.35 $W m^{-2}$) with peaks of 150 $W m^{-2}$ (150 $W m^{-2}$) on dry days (wet days). Furthermore, the new cooling tower scheme improves the model performance of surface temperature and humidity. Maximum and minimum average temperature errors improve by 2°–3°C, especially on dry days. Along the boundary layer, model performance of the vertical structure in the rural areas is much better represented by the model than in urban areas. RMSE of surface temperatures simulated by EC in urban areas is improved, especially on wet days, for which the RMSE is reduced to 0.45°C (Table 3). For humidity, the model performance is also improved by EC, and the RMSE of humidity is reduced to 2.82 g kg^{-1} on dry days and 2.00 g kg^{-1} on wet days. In addition, model performance of sensible and latent heat fluxes is clearly improved by EC. RMSE of latent heat flux is reduced by about 50%, and RMSE of sensible heat flux is reduced by 10% in EC. As a consequence of

TABLE 3. RMSE for 2-m temperature (°C), specific humidity (g kg^{-1}), and sensible and latent heat flux (W m^{-2}) for dry and wet days for the CTL and EC simulations.

RMSE	Temperature	Humidity	Sensible heat flux	Latent heat flux
CTL dry day	1.31	3.91	123.34	73.22
EC dry day	1.01	2.82	105.45	20.56
CTL wet day	1.36	3.43	90.33	57.45
EC wet day	0.45	2.00	85.34	35.78

this study, this EC scheme has been adopted in a real-time RMAPS-Urban system in Beijing.

Although model performance of latent heat flux has been improved by the cooling tower scheme, there is room for improvement when compared with the observations. Urban evaporation effects that also affect the latent heat flux in urban areas (e.g., urban hydrological processes, evaporation from impervious surface, urban oasis effect, green roof) are not considered in the current BEP+BEM. In addition, the results could be different using a different PBL scheme.

Acknowledgments. The authors thank the anonymous reviewers for constructive comments. This work was supported by National Natural Science Foundation of China (Grant 41705090), National Natural Science Foundation of China (Grant 41705088), and the Ministry of Science and Technology of China (Grant IUMKY201804 and IUMKY201902).

REFERENCES

Adnot, J., and Coauthors, 2003: Energy efficiency and certification of central air conditioners (EECCAC): Final report—April 2003. ARMINES Study for the D.G. Transportation-Energy (DGTREN) of the Commission of the E.U., 200 pp.

Akbari, H., and S. Konopacki, 2004: Energy savings of heat-island reduction strategies in Toronto, Canada. *Energy*, **29**, 191–210, https://doi.org/10.1016/j.energy.2003.09.004.

——, M. Pomerantz, and H. Taha, 2001: Cool surfaces and shade trees to reduce energy use and improve air quality in urban areas. *Sol. Energy*, **70**, 295–310, https://doi.org/10.1016/S0038-092X(00)00089-X.

Allen, L., F. Lindberg, and C. S. B. Grimmond, 2011: Global to city scale urban anthropogenic heat flux: Model and variability. *Int. J. Climatol.*, **31**, 1990–2005, https://doi.org/10.1002/joc.2210.

Barlage, M., S. Miao, and F. Chen, 2016: Impact of physics parameterizations on high-resolution weather prediction over two Chinese megacities. *J. Geophys. Res. Atmos.*, **121**, 4487–4498, https://doi.org/10.1002/2015JD024450.

Block, A., K. Keuler, and E. Schaller, 2004: Impacts of anthropogenic heat on regional climate patterns. *Geophys. Res. Lett.*, **31**, L12211, https://doi.org/10.1029/2004GL019852.

Bougeault, P., and P. Lacarrere, 1989: Parameterization of orography-induced turbulence in a mesobeta–scale model. *Mon. Wea. Rev.*, **117**, 1872–1890, https://doi.org/10.1175/1520-0493(1989)117<1872:POOITI>2.0.CO;2.

Chen, F., and Coauthors, 2011: The integrated WRF/urban modelling system: Development, evaluation, and applications to urban environmental problems. *Int. J. Climatol.*, **31**, 273–288, https://doi.org/10.1002/joc.2158.

Crutzen, P. J., 2004: New directions: The growing urban heat and pollution "island" effect—Impact on chemistry and climate. *Atmos. Environ.*, **38**, 3539–3540, https://doi.org/10.1016/j.atmosenv.2004.03.032.

de Munck, C., and Coauthors, 2013: How much can air conditioning increase air temperatures for a city like Paris, France? *Int. J. Climatol.*, **33**, 210–227, https://doi.org/10.1002/joc.3415.

Dudhia, J., 1989: Numerical study of convection observed during the winter monsoon experiment using a mesoscale two-dimensional model. *J. Atmos. Sci.*, **46**, 3077–3107, https://doi.org/10.1175/1520-0469(1989)046<3077:NSOCOD>2.0.CO;2.

Fan, S., 2015: Assessment report of regional high resolution model (BJ-RUCv3.0). IUM Tech. Note IUM/2015-1, 21 pp.

Feng, J., Y. Wang, Z. Ma, and Y. Liu, 2012: Simulating the regional impacts of urbanization and anthropogenic heat release on climate across China. *J. Climate*, **25**, 7187–7203, https://doi.org/10.1175/JCLI-D-11-00333.1.

Flanner, M. G., 2009: Integrating anthropogenic heat flux with global climate models. *Geophys. Res. Lett.*, **36**, L02801, https://doi.org/10.1029/2008GL036465.

González, J. E., and A. J. Bula-Silvera, 2017: Conventional mechanical systems for efficient heating, ventilating, and air conditioning systems. *Energy Systems*, Vol. I, *Handbook of Integrated and Sustainable Buildings Equipment and Systems*, ASME Press, https://doi.org/10.1115/1.861271_ch3.

Gutiérrez, E., J. Gonzalez, A. Martilli, R. Bornstein, and M. Arend, 2015: Simulations of a heat wave event in New York City using a multilayer urban parameterization. *J. Appl. Meteor. Climatol.*, **54**, 283–301, https://doi.org/10.1175/JAMC-D-14-0028.1.

Hassid, S., M. Santamouris, N. Papanikolaou, A. Linardi, N. Klitsikas, C. Georgakis, and D. N. Assimakopoulos, 2000: The effect of the Athens heat island on air conditioning load. *Energy Build.*, **32**, 131–141, https://doi.org/10.1016/S0378-7788(99)00045-6.

Haub, C., 2010: World population data sheet. Population Reference Bureau, 19 pp., https://www.prb.org/wp-content/uploads/2010/11/10wpds_eng.pdf.

He, X., W. Jiang, Y. Chen, and G. Liu, 2007: Numerical simulation of the impacts of anthropogenic heat on the structure of the urban boundary layer. *Chin. J. Geophys.*, **50**, 75–83, https://doi.org/10.1002/cjg2.1012.

Hinkel, K. M., and F. E. Nelson, 2007: Anthropogenic heat island at Barrow, Alaska, during winter: 2001–2005. *J. Geophys. Res.*, **112**, D06118, https://doi.org/10.1029/2006JD007837.

Hsieh, C.-M., T. Aramaki, and K. Hanaki, 2007: The feedback of heat rejection to air conditioning load during the nighttime in

subtropical climate. *Energy Build.*, **39**, 1175–1182, https://doi.org/10.1016/j.enbuild.2006.06.016.

Hu, Y., W. Dong, and Y. He, 2010: Impact of land surface forcings on mean and extreme temperature in eastern China. *J. Geophys. Res.*, **115**, D19117, https://doi.org/10.1029/2009JD013368.

Ichinose, T., K. Shimodozono, and K. Hanaki, 1999: Impact of anthropogenic heat on urban climate in Tokyo. *Atmos. Environ.*, **33**, 3897–3909, https://doi.org/10.1016/S1352-2310(99)00132-6.

Kain, J. S., 2004: The Kain–Fritsch convective parameterization: An update. *J. Appl. Meteor.*, **43**, 170–181, https://doi.org/10.1175/1520-0450(2004)043<0170:TKCPAU>2.0.CO;2.

Kalnay, E., and M. Cai, 2003: Impact of urbanization and land-use change on climate. *Nature*, **423**, 528–531, https://doi.org/10.1038/nature01675.

——, ——, H. Li, and J. Tobin, 2006: Estimation of the impact of land-surface forcings on temperature trends in eastern United States. *J. Geophys. Res.*, **111**, D06106, https://doi.org/10.1029/2005JD006555.

Kolokotroni, M., I. Giannitsaris, and R. Watkins, 2006: The effect of the London urban heat island on building summer cooling demand and night ventilation strategies. *Sol. Energy*, **80**, 383–392, https://doi.org/10.1016/j.solener.2005.03.010.

Kusaka, H., and F. Kimura, 2004: Coupling a single-layer urban canopy model with a simple atmospheric model: Impact on urban heat island simulation for an idealized case. *J. Meteor. Soc. Japan*, **82**, 67–80, https://doi.org/10.2151/jmsj.82.67.

——, H. Kondo, Y. Kikegawa, and F. Kimura, 2001: A simple single-layer urban canopy model for atmospheric models: Comparison with multi-layer and slab models. *Bound.-Layer Meteor.*, **101**, 329–358, https://doi.org/10.1023/A:1019207923078.

Li, Q., H. Zhang, X. Liu, and J. Huang, 2004: Urban heat island effect on annual mean temperature during the last 50 years in China. *Theor. Appl. Climatol.*, **79**, 165–174, https://doi.org/10.1007/s00704-004-0065-4.

Li, Y., L. Zhu, X. Zhao, S. Li, and Y. Yan, 2013: Urbanization impact on temperature change in China with emphasis on land cover change and human activity. *J. Climate*, **26**, 8765–8780, https://doi.org/10.1175/JCLI-D-12-00698.1.

Liang, X., and Coauthors, 2018: SURF: Understanding and predicting urban convection and haze. *Bull. Amer. Meteor. Soc.*, **99**, 1391–1413, https://doi.org/10.1175/BAMS-D-16-0178.1.

Liao, J., L. Tang, G. Shao, Q. Qiu, C. Wang, S. Zheng, and X. Su, 2014: A neighbor decay cellular automata approach for simulating urban expansion based on particle swarm intelligence. *Int. J. Geogr. Inf. Sci.*, **28**, 720–738, https://doi.org/10.1080/13658816.2013.869820.

Martilli, A., A. Clappier, and M. W. Rotach, 2002: An urban surface exchange parameterization for mesoscale models. *Bound.-Layer Meteor.*, **104**, 261–304, https://doi.org/10.1023/A:1016099921195.

Miao, S. G., F. Chen, M. A. LeMone, M. Tewari, Q. Li, and Y. Wang, 2009: An observation al and modeling study of characteristics of urban heat island and boundary layer structures in Beijing. *J. Appl. Meteor. Climatol.*, **48**, 484–501, https://doi.org/10.1175/2008JAMC1909.1.

Mlawer, E. J., S. J. Taubman, P. D. Brown, M. J. Iacono, and S. A. Clough, 1997: Radiative transfer for inhomogeneous atmospheres: RRTM, a validated correlated-*k* model for the longwave. *J. Geophys. Res.*, **102**, 16 663–16 682, https://doi.org/10.1029/97JD00237.

Narumi, D., A. Kondo, and Y. Shimoda, 2009: Effects of anthropogenic heat release upon the urban climate in a Japanese megacity. *Environ. Res.*, **109**, 421–431, https://doi.org/10.1016/j.envres.2009.02.013.

Ohashi, Y., Y. Genchi, H. Kondo, Y. Kikegawa, H. Yoshikado, and Y. Hirano, 2007: Influence of air-conditioning waste heat on air temperature in Tokyo during summer: Numerical experiments using an urban canopy model coupled with a building energy model. *J. Appl. Meteor. Climatol.*, **46**, 66–81, https://doi.org/10.1175/JAM2441.1.

Olivo, Y., A. Hamidi, and P. Ramamurthy, 2017: Spatio-temporal variability in building energy use in New York City. *Energy*, **141**, 1393–1401, https://doi.org/10.1016/j.energy.2017.11.066.

Pleim, J. E., 2007: A combined local and non-local closure model for the atmospheric boundary layer. Part I: Model description and testing. *J. Appl. Meteor. Climatol.*, **46**, 1383–1395, https://doi.org/10.1175/JAM2539.1.

Roth, M., 2007: Review of urban climate research in (sub) tropical regions. *Int. J. Climatol.*, **27**, 1859–1873, https://doi.org/10.1002/joc.1591.

Sailor, D. J., 2011: A review of methods for estimating anthropogenic heat and moisture emissions in the urban environment. *Int. J. Climatol.*, **31**, 189–199, https://doi.org/10.1002/joc.2106.

——, A. Brooks, M. Hart, and S. Heiple, 2007: A bottom-up approach for estimating latent and sensible heat emissions from anthropogenic sources. *Seventh Symp. on the Urban Environment*, San Diego, CA, Amer. Meteor. Soc., 3.6, https://ams.confex.com/ams/pdfpapers/127290.pdf.

Salamanca, F., and A. Martilli, 2010: A new building energy model coupled with an urban canopy parameterization for urban climate simulations—Part II. Validation with one dimension off-line simulations. *Theor. Appl. Climatol.*, **99**, 345–356, https://doi.org/10.1007/s00704-009-0143-8.

——, ——, M. Tewari, and F. Chen, 2011: A Study of the urban boundary layer using different urban parameterizations and high-resolution urban canopy parameters with WRF. *J. Appl. Meteor. Climatol.*, **50**, 1107–1128, https://doi.org/10.1175/2010JAMC2538.1.

——, M. Georgescu, A. Mahalov, M. Moustaoui, and M. Wang, 2014: Anthropogenic heating of the urban environment due to air conditioning. *J. Geophys. Res. Atmos.*, **119**, 5949–5965, https://doi.org/10.1002/2013JD021225.

Skamarock, W. C., and Coauthors, 2008: A description of the Advanced Research WRF version 3. NCAR Tech. Note NCAR/TN-475+STR, 113 pp., https://doi.org/10.5065/D68S4MVH.

Stull, R., 2011: Wet-bulb temperature from relative humidity and air temperature. *J. Appl. Meteor. Climatol.*, **50**, 2267–2269, https://doi.org/10.1175/JAMC-D-11-0143.1.

Thompson, G., R. Rasmussen, and K. Manning, 2004: Explicit forecasts of winter precipitation using an improved bulk microphysics scheme. Part I: Description and sensitivity analysis. *Mon. Wea. Rev.*, **132**, 519–542, https://doi.org/10.1175/1520-0493(2004)132<0519:EFOWPU>2.0.CO;2.

Wen, Y., and Z. Lian, 2009: Influence of air conditioners utilization on urban thermal environment. *Appl. Therm. Eng.*, **29**, 670–675, https://doi.org/10.1016/j.applthermaleng.2008.03.039.

Yang, B., Y. Zhang, and Y. Qian, 2012: Simulation of urban climate with high-resolution WRF model: A case study in Nanjing, China. *Asia-Pac. J. Atmos. Sci.*, **48**, 227–241, https://doi.org/10.1007/s13143-012-0023-5.

Zhang, G., M. Cai, and A. Hu, 2013: Energy consumption and the unexplained winter warming over northern Asia and North

America. *Nat. Climate Change*, **3**, 466–470, https://doi.org/10.1038/nclimate1803.

Zhang, Y., S. Miao, Y. Dai, and Y. H. Liu, 2013: Numerical simulation of characteristics of summer clear day boundary layer in Beijing and the impact of urban underlying surface on sea breeze (in Chinese). *Chin. J. Geophys.*, **56**, 2558–2573.

——, ——, ——, and R. Bornstein, 2017: Numerical simulation of urban land surface effects on summer convective rainfall under different UHI intensity in Beijing. *J. Geophys. Res. Atmos.*, **122**, 7851–7868, https://doi.org/10.1002/2017JD026614.

Zheng, S., and S. Liu, 2008: Urbanization effect on climate in Beijing. *Climate Environ. Res.*, **13**, 123–133.

Zheng, Y., S. Miao, Q. Zhang, and Y. Bao, 2015: Improvements of building energy model and anthropogenic heat release from cooling system. *Plateau Meteor.*, **34**,786–796, https://doi.org/10.7522/j.issn.1000-0534.2014.00035.

Zhou, L. M., R. E. Dickinson, Y. Tian, J. Fang, Q. Li, R. K. Kaufmann, C. J. Tucker, and R. B. Myneni, 2004: Evidence for a significant urbanization effect on climate in China. *Proc. Natl. Acad. Sci. USA*, **101**, 9540–9544, https://doi.org/10.1073/pnas.0400357101.